Molecular Therapy
Nucleic Acids
Original Article

# Evaluation of Antisense Oligonucleotides Targeting ATXN3 in SCA3 Mouse Models

Lauren R. Moore,[1,3] Gautam Rajpal,[1,3] Ian T. Dillingham,[1] Maya Qutob,[1] Kate G. Blumenstein,[1] Danielle Gattis,[2] Gene Hung,[2] Holly B. Kordasiewicz,[2] Henry L. Paulson,[1] and Hayley S. McLoughlin[1]

[1]Department of Neurology, University of Michigan, Ann Arbor, MI 48109-2200, USA; [2]Ionis Pharmaceuticals, Carlsbad, CA 92008, USA

**The most common dominantly inherited ataxia, spinocerebellar ataxia type 3 (SCA3), is an incurable neurodegenerative disorder caused by a CAG repeat expansion in the *ATXN3* gene that encodes an abnormally long polyglutamine tract in the disease protein, ATXN3. Mice lacking ATXN3 are phenotypically normal; hence, disease gene suppression offers a compelling approach to slow the neurodegenerative cascade in SCA3. Here we tested antisense oligonucleotides (ASOs) that target human *ATXN3* in two complementary mouse models of SCA3: yeast artificial chromosome (YAC) MJD-Q84.2 (Q84) mice expressing the full-length human *ATXN3* gene and cytomegalovirus (CMV) MJD-Q135 (Q135) mice expressing a human *ATXN3* cDNA. Intracerebroventricular injection of ASOs resulted in widespread delivery to the most vulnerable brain regions in SCA3. In treated Q84 mice, three of five tested ASOs reduced disease protein levels by >50% in the diencephalon, cerebellum, and cervical spinal cord. Two ASOs also significantly reduced mutant ATXN3 in the mouse forebrain and resulted in no signs of astrogliosis or microgliosis. In Q135 mice expressing a single ATXN3 isoform via a cDNA transgene, ASOs did not result in similar robust ATXN3 silencing. Our results indicate that ASOs targeting full-length human *ATXN3* would likely be well tolerated and could lead to a preventative therapy for SCA3.**

## INTRODUCTION

Spinocerebellar ataxia type 3 (SCA3) is one of nine polyglutamine expansion diseases and the most common dominantly inherited ataxia in the world.[1] While certain symptoms in SCA3 may respond to symptomatic therapy, there is still no effective treatment for this relentlessly progressive and fatal neurodegenerative disease. SCA3 is caused by a CAG repeat expansion in the *ATXN3* gene, resulting in an abnormally long polyglutamine stretch in the encoded ATXN3 protein. Because expression of mutant ATXN3 is an early and necessary step in disease pathogenesis, strategies to reduce expression of the disease gene itself are high on the list of potential therapies.[2–6] Mice lacking the homologous *Atxn3* gene appear normal, suggesting that human ATXN3 may not be an essential protein.[7] Thus, lowering expression of the disease gene in SCA3 may be well tolerated. Additionally, in a doxycycline-regulatable transgenic mouse model of SCA3, reducing production of mutant *ATXN3* transcripts via doxycycline treatment beginning at 9 weeks eliminated disease features.[8] This result implies that treatment at an early symptomatic stage, prior to extensive irreversible tissue damage, holds promise for SCA3 therapy.

Among gene suppression approaches, viral-mediated gene therapy has been explored by us and others in mouse models of SCA3. In transgenic mice expressing the full human *ATXN3* disease gene, bilateral delivery of small interfering RNA targeting *ATXN3* to the deep cerebellar nuclei (DCN) was well tolerated and led to sustained suppression of mutant ATXN3 in the cerebellum,[4] but it did not rescue motor deficits and the lifespan in these mice.[3] Because degeneration in patients with SCA3 extends beyond the cerebellum to include selective brainstem nuclei, the striatum, and the thalamus, effective gene therapy for SCA3 may require broader CNS delivery.[9] Additional RNAi studies targeting *ATXN3* succeeded in preventing motor deficits in a lentiviral mouse model of SCA3 in which expanded *ATXN3* was virally delivered to the cerebellum,[2,5] but these studies have not yet been replicated in mouse models expressing mutant ATXN3 throughout the CNS.

Antisense oligonucleotides (ASOs) represent a therapeutic non-viral gene suppression approach that is increasingly being tested in neurodegenerative and metabolic disorders. ASOs are short single strands of chemically modified oligonucleotides that selectively bind complementary mRNA via Watson-Crick hybridization to drive RNase H-mediated cleavage of the targeted mRNA.[10] ASOs targeting disease-causing genes have been tested in rodent models of various neurodegenerative disorders and have advanced into human clinical trials, including ASOs for spinal muscular atrophy (SMA), familial amyotrophic lateral sclerosis (ALS), and Huntington's disease (HD).[11–16] ASOs targeting *ATXN3* have been developed and tested in cellular and in vivo models of SCA3, with some limitations.[6,17–21]

Received 10 March 2017; accepted 6 April 2017;
http://dx.doi.org/10.1016/j.omtn.2017.04.005.

[3]These authors contributed equally to this work.

**Correspondence:** Henry L. Paulson, MD, PhD, Department of Neurology, University of Michigan, A. Alfred Taubman Biomedical Sciences Research Building, Room 4001, 109 Zina Pitcher Place, Ann Arbor, MI 48109-2200, USA.
**E-mail:** henryp@umich.edu
**Correspondence:** Hayley S. McLoughlin, PhD, Department of Neurology, University of Michigan, A. Alfred Taubman Biomedical Sciences Research Building, Room 4178, 109 Zina Pitcher Place, Ann Arbor, MI 48109-2200, USA.
**E-mail:** hayleymc@umich.edu

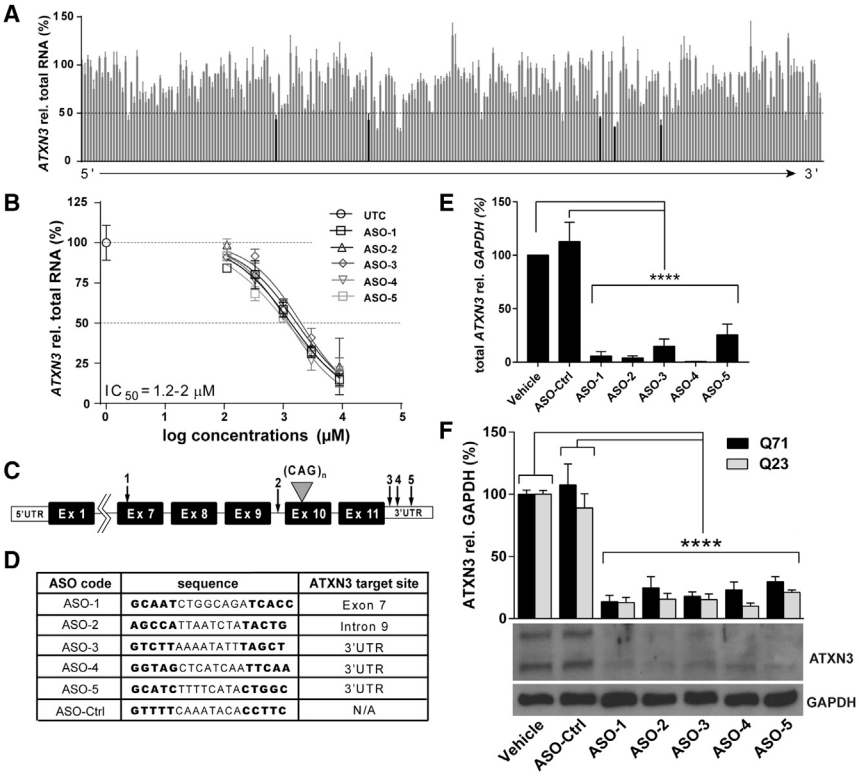


**Figure 1. Identification of Human ATXN3 Antisense Oligonucleotides**

(A) Screen of ASOs complementary to human *ATXN3* in HEPG2 cells. 2 μM ASO was electroporated into HEPG2 cells; 24 hr post-treatment, *ATXN3* mRNA levels were quantified by qPCR and normalized to total RNA levels. Data expressed as the percent of untransfected control cells. ASOs listed in order of relative binding site on *ATXN3* transcript (5′ to 3′). Five ASOs characterized further are noted in black. (B) Dose response of top five ASOs in HEPG2 cells. $IC_{50}$s calculated from four-point non-linear fit dose-response curve. (C) Schematic of anti-*ATXN3* ASO target sites on the human *ATXN3* transcript. (D) Anti-*ATXN3* ASOs and the non-specific ASO-Ctrl nucleotide sequence possess a 5-8-5 MOE gapmer design in which an 8-mer block of unmodified deoxynucleotides is flanked by 5-mer blocks of 2′-O-methoxyethyl (MOE)-modified ribonucleotides indicated in bold. (E) Total *ATXN3* transcript levels in SCA3 patient fibroblasts 48 hr after transfection with anti-*ATXN3* ASOs (4 μM), ASO-Ctrl, or vehicle. Data (mean ± SEM) are reported relative to fibroblasts treated with vehicle alone (n = 6 per group). One-way ANOVA statistical analysis performed with the post hoc Tukey test (****$p < 0.0001$). (F) Immunoblotting and quantification of expanded (Q71) and wild-type (Q23) ATXN3 protein in SCA3 patient fibroblasts 72 hr after transfection with anti-*ATXN3* ASOs, ASO-Ctrl, or vehicle. Data (mean ± SEM) are reported relative to fibroblasts treated with vehicle (n = 6 per group). One-way ANOVA performed with the post hoc Tukey test (****$p < 0.0001$).

Allele-specific ASOs that selectively target the CAG repeat expansion in an effort to preserve wild-type ATXN3 function have been tested in SCA3 cellular models, but the ubiquity of CAG repeats in the human transcriptome may pose challenging off-target effects.[17–20] Splice-switching ASOs have also been developed but failed to achieve greater than 50% knockdown of full-length mutant ATXN3 in the ASO-treated mouse cerebellum and did not preserve the deubiquitinating function of ATXN3.[6,21]

Here we evaluate the efficiency of non-allele-specific ASOs targeting human *ATXN3* in two complementary transgenic mouse models of SCA3: the yeast artificial chromosome (YAC) MJD-Q84.2 (Q84) model expressing the full-length human *ATXN3* disease gene with 84 CAG repeats, and the cytomegalovirus (CMV) MJD-Q135 (Q135) model expressing a single human ATXN3 isoform from an *ATXN3* cDNA with 135 CAG repeats.[22,23] Overall, two candidate ASOs led to widespread delivery and efficient silencing of mutant human ATXN3 with no immune response in the Q84 mouse model of SCA3. Our results support the continued development of anti-*ATXN3* ASOs as therapy for SCA3.

## RESULTS

### Identification of Human ATXN3 ASOs

To identify active *ATXN3* ASOs, ASOs complementary to human *ATXN3* coding and non-coding regions were screened at a single dose in HEPG2 cells, a human cell line that expresses *ATXN3* transcripts. Following ASO treatment, the ability of the ASOs to suppress normal *ATXN3* transcripts was quantified (Figure 1A). The most active ASOs were subjected to dose response to determine their in vitro median inhibitory concentration ($IC_{50}$), and from these, five anti-*ATXN3* ASOs with similar $IC_{50}$s (1.2–2 μM) (Figure 1B) targeting coding or non-coding regions of the human *ATXN3* transcript were selected for further characterization (Figure 1C). All five anti-*ATXN3* ASOs, denoted ASO-1 through ASO-5, as well as a scrambled control ASO (ASO-Ctrl), shared a 5-8-5 2′-O-methoxyethyl (MOE) gapmer design with phosphorothioate backbone modifications, as well as 5-mer blocks of MOE-modified ribonucleotides flanking an 8-mer block of deoxynucleotides without sugar modifications (Figure 1D). This MOE gapmer design has previously been shown to increase stability and potency of ASOs and is the design taken into clinical trials for ALS and HD.[14,24,25]

### Anti-*ATXN3* ASOs Suppress Mutant and Wild-Type ATXN3 in SCA3 Patient Fibroblasts

To assess target efficiency of ASOs in patient cells, SCA3 patient-derived fibroblasts (GM06153) were transfected with ASO candidates, ASO-Ctrl, or PBS vehicle alone. GM06153 fibroblasts are heterozygous for the mutant *ATXN3* allele harboring a CAG expansion with 71 repeats and a non-pathological repeat of 23. Cells were transfected with ASOs (4 μM) and harvested 48 or 72 hr later for RNA or protein assessment, respectively. The experimenter was blinded to treatments prior to testing. All five ASOs targeting *ATXN3* robustly

suppressed ATXN3 transcript and protein levels ($p < 0.0001$) (Figures 1E and 1F). ASOs suppressed expanded and wild-type ATXN3 similarly, indicating no allele selectivity. Only one of the five ASOs, ASO-4, exhibited any toxicity following transfection, with visible detachment of a fraction of treated cells (data not shown).

### In Vivo Assessment of ASOs in Hemizygous Q84 Transgenic Mice

All five ASO candidates were subjected to in vivo tolerability screening in non-transgenic mice. Animals received a single 700 μg intracerebroventricular (i.c.v.) bolus injection into the right lateral ventricle, and animals were monitored for 7 weeks after injection. Animals were weighed and examined weekly. ASO-treated animals did not exhibit any overt behavioral deficits or differences in body weight compared to PBS-treated controls (data not shown). One ASO-2-treated animal died during surgery, but this was deemed non-drug related. At the conclusion of the study, *Iba1* mRNA in the cortex immediately adjacent to the injection site was quantified as a surrogate for microglial activation, and no significant changes were observed between ASO groups and PBS (data not shown). Thus, all five ASO candidates were selected for further in vivo assessment in the Q84 transgenic mouse model of SCA3.

Hemizygous Q84 mice express the full-length human *ATXN3* gene with a pathogenic expansion of 84 CAG repeats at near endogenous ATXN3 expression levels, and thus represent a biologically relevant model of the human disease.[23] This mouse line has been validated in previous SCA3 gene therapy studies.[3,23] Neuropathological features of SCA3, such as enhanced mutant ATXN3 nuclear burden and the formation of cytoplasmic and intranuclear inclusions in neurons, are apparent as early as 6 weeks of age in hemizygous Q84 mice.[3,23]

To assess whether anti-*ATXN3* ASO intervention early in the disease process can suppress accumulation of mutant ATXN3 protein in vivo, we injected 8-week-old sex-matched hemizygous Q84 mice with a single stereotaxic i.c.v. bolus injection into the right lateral ventricle. Each mouse received 500 μg ASOs diluted in 10 μL PBS at an injection rate of 0.5 μL/s to enhance ASO spread.[11] Wild-type littermates were also injected with PBS vehicle for comparison. Mice were subsequently monitored according to University of Michigan Committee on Use and Care of Animals (UCUCA) guidelines, with no post-surgical adverse events or deaths occurring. Treated brains were harvested 4 weeks after injection and bisected along the midline. The left hemisphere contralateral to injection was further dissected into the forebrain, cerebellum, diencephalon, and cervical spinal cord for protein and RNA analysis, while the right hemisphere ipsilateral to the injection site was processed for immunohistochemical (IHC) analysis (Figure 2A). All treatment groups were blinded to the experimenter prior to analysis.

In SCA3, many neuronal populations in the diencephalon appear selectively vulnerable and exhibit ATXN3-positive aggregate pathology.[26,27] Four of the five ASO candidates significantly reduced mutant *ATXN3* transcripts in the diencephalon relative to vehicle-treated mice, assessed by qRT-PCR (Figure 2B). Two ASOs targeting the 3′-UTR of *ATXN3*, ASO-4 and ASO-5, achieved the greatest transcript reduction in the diencephalon, reducing mutant *ATXN3* transcript levels by 63.8% ± 6.8% ($p < 0.001$) and 83.9% ± 4.6% ($p < 0.0001$), respectively, relative to vehicle-treated mice. ASO-1- and ASO-2-treated mice also showed significant transcript reduction in the diencephalon (58.2% ± 24.5% and 56.4% ± 23.7%, respectively; $p < 0.01$).

Suppression of mutant ATXN3 protein expression was assessed by western blot of left forebrain, cerebellum, diencephalon, and cervical spinal cord protein lysates from treated mice (Figures 2C and 2D). Mirroring the reduction in diencephalon transcript levels, mutant ATXN3 protein levels were significantly reduced in the diencephalon, cerebellum, and cervical spinal cord of mice treated with ASO-2 ($p < 0.05$), ASO-4 ($p < 0.05$), or ASO-5 ($p < 0.01$). Additionally, a significant mutant ATXN3 reduction was found in forebrain lysates of ASO-2-treated ($p < 0.05$) and ASO-5-treated ($p < 0.01$) mice. In ASO-1-treated mice, high variability in mutant ATXN3 protein levels was observed in all analyzed brain regions, with four of six mice exhibiting mutant ATXN3 suppression of more than 50% relative to vehicle-treated mice, while the remaining two mice exhibited no decrease in mutant ATXN3 levels.

Levels of high molecular weight (HMW) ATXN3 aggregate species resolvable by SDS-PAGE were also quantified in diencephalon protein lysates from treated mice. HMW ATXN3 levels were significantly reduced by 63.7% ± 7.7% and 68.5 ± 7.3% in the diencephalon of mice treated with ASO-2 ($p < 0.05$) and ASO-5 ($p < 0.05$), respectively, relative to vehicle-treated Q84 mice (Figures 2E and 2F). HMW ATXN3 trended toward a decrease in ASO-4-treated mice, but failed to reach significance due to variability across mice ($p = 0.09$).

Analysis of diencephalon protein lysates also revealed a significant decrease in endogenous murine ATXN3 protein in Q84 mice treated with ASO-1 (42.9% ± 8.3%; $p < 0.05$), ASO-2 (40.2% ± 14.4%; $p < 0.05$), ASO-4 (42.0% ± 12.0%; $p < 0.05$), and ASO-5 (82.6% ± 9.3%; $p < 0.0001$) relative to vehicle-treated Q84 mice (Figure 2G). Of the five ASOs tested, only ASO-5 was expected to directly target the murine mRNA transcript due to species conservation of the target sequence between the human and murine *ATXN3* gene (Figure 2B). Previous studies have shown that mutant expanded ATXN3 can oligomerize with non-expanded ATXN3, leading to increased retention of both pathogenic and non-pathogenic ATXN3 proteins.[28] Thus, a reduction of murine ATXN3 protein may reflect decreased interactions with the mutant protein leading to normalization of the protein clearance rate. Furthermore, vehicle-treated Q84 mice exhibited paradoxical decreases in *Atxn3* transcript levels ($p < 0.05$) (Figure 2B) and increased endogenous protein levels of murine ATXN3 relative to vehicle-treated wild-type animals ($p < 0.001$) (Figure 2G). This may reflect a negative regulatory feedback effect on *Atxn3* transcription in disease.

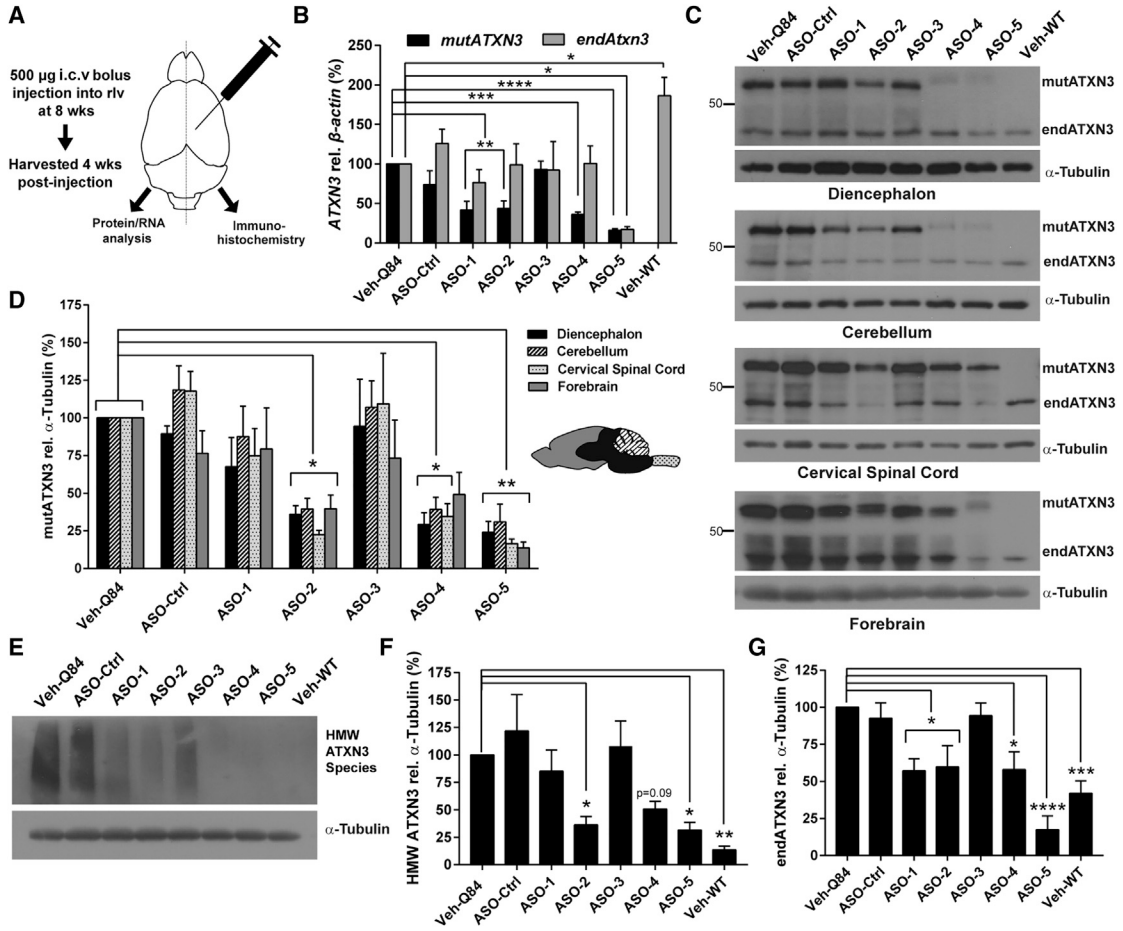


**Figure 2. In Vivo Suppression of Mutant ATXN3 by Anti-*ATXN3* ASOs in Q84 Mice, a YAC Transgenic Mouse Model of SCA3**

(A) Schematic of anti-*ATXN3* ASO trial design. Sex-matched hemizygous Q84 mice received a single i.c.v. bolus injection of 500 µg ASO or vehicle into the right lateral ventricle (rlv) at 8 weeks of age. Brains were harvested and dissected 4 weeks later for RNA, protein, and immunohistochemical analysis. (B) Quantification of endogenous *Atxn3* (*endAtxn3*) and mutant *ATXN3* (*mutATXN3*) transcripts in the diencephalon of vehicle- (Veh-Q84 and Veh-WT), ASO-Ctrl-, and anti-*ATXN3* ASO-treated mice. (C) Representative western blots of mutant ATXN3 (mutATXN3) and endogenous ATXN3 (endATXN3) protein expression in major brain regions of treated mice. (D) Quantification of mutATXN3 protein expression in major brain regions of treated mice. (E and F) Representative western blot (E) and quantification of high molecular weight (HMW) ATXN3 species in the diencephalon of treated mice (F). (G) Quantification of endATXN3 protein expression in the diencephalon of treated mice. Data (mean ± SEM) are reported relative to mice treated with vehicle (n = 6 per group). One-way ANOVA performed with the post hoc Dunnett test (*$p < 0.05$; **$p < 0.01$; ***$p < 0.001$; ****$p < 0.0001$). WT, wild type.

ASO delivery and potency in disease-relevant neuronal populations were further investigated with anti-ATXN3 and anti-ASO immunofluorescence on brain sections from the injected hemisphere. Four weeks following injection, all ASOs were widely distributed throughout the brain, including in the striatum, cerebellar lobules, DCN, pons, hippocampus, and cerebral cortex (Figure 3A). Areas of high vulnerability in SCA3, including the DCN and pontine nuclei, exhibited high levels of delivered ASO and, correspondingly, clearly decreased levels of ATXN3 expression in these regions (Figures 3B and 3C). Furthermore, in SCA3, ATXN3 abnormally accumulates in neuronal nuclei. Q84 mice treated with ASO-2, ASO-4, and ASO-5 exhibited markedly decreased neuronal nuclear ATXN3 staining in the DCN and pons ($p < 0.0001$), two neuronal populations that are highly affected in SCA3 (Figure 4). ASO-5 led to the greatest reduction in ATXN3 immunostaining in the DCN and pons, likely due to the fact that it is the only tested ASO that targets both human and murine *ATXN3* transcripts.

To investigate the tolerability and safety of ASOs in vivo, we assessed transcript levels of markers of immune-reactive cell types—namely, astrocytes (*Gfap*) and microglia (*Iba1*)—in the diencephalon of treated mice. *Gfap* levels were not altered in mice treated with ASO-2 or ASO-5 but were significantly increased in mice treated with ASO-4 ($p < 0.05$) (Figure 5A), the only ASO that also exhibited cellular toxicity in patient fibroblasts. *Iba1* transcript levels were not increased in the diencephalon of ASO-2- or ASO-4-treated mice,

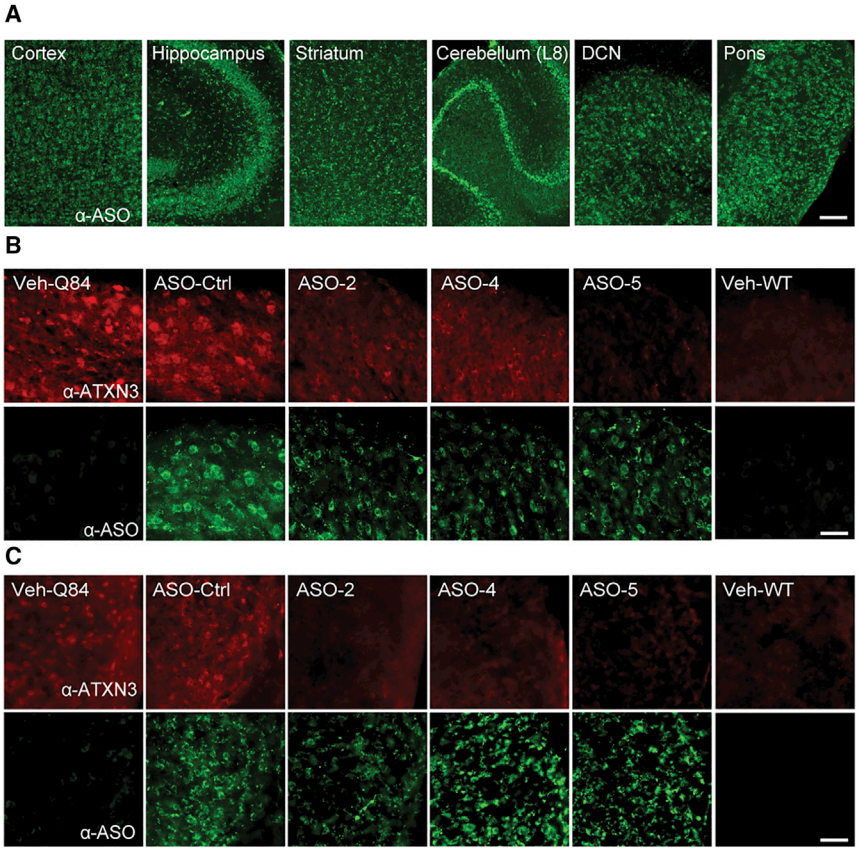


**Figure 3. Anti-*ATXN3* ASOs Distribute Widely throughout the CNS and Suppress ATXN3 Protein Expression in Q84 Mice**

(A) Representative immunofluorescence images of ASO (green) distributed throughout key SCA3-affected brain regions in Q84 hemizygous mice 4 weeks after injection. (B and C) Representative immunofluorescence images of ASO-mediated (green) suppression of ATXN3 (red) in deep cerebellar nuclei (DCN) (B) and pontine nuclei (C) of Q84 hemizygous mice 4 weeks post-treatment. Scale bars represent 200 μm in (A) and 50 μm in (B) and (C).

although *Iba1* levels trended toward an increase in ASO-4-treated mice, mirroring the increased *Gfap* transcript levels in ASO-4-treated mice and further supporting the possible toxicity of this ASO. Intriguingly, ASO-5 treatment of Q84 mice actually led to a significant decrease ($p < 0.05$) in *Iba1* transcript levels in the diencephalon relative to vehicle- or ASO-Ctrl-treated mice (Figure 5B). This result suggests a possible rescue of disease-related neuroinflammatory changes in SCA3 mice by ASO-5 treatment.

Immunofluorescence assessment of reactive astrocytes and microglia was performed throughout the brain of the injected hemisphere. Unexpectedly, we noted a discrepancy in astrocyte-microglia patterning in the DCN of mice treated with ASO-4, specifically. The DCN typically exhibits a pattern of GFAP-positive astrocytes forming a rim around the nucleus, which in turn is dominated by IBA1-positive microglia, with little overlap between the two cell types. However, ASO-4-treated mice consistently demonstrated infiltration of astrocytes from the surrounding region into the DCN, indicative of possible ASO-4 toxicity leading to inflammatory changes in this brain region (Figure 5C). All mice, including vehicle-, ASO-Ctrl-, and anti-ATXN3 ASO-treated mice, exhibited similar local gliosis immediately surrounding the injection site (data not shown) but, consistent with our earlier screens in wild-type mice, there were no differences in IBA1 or GFAP expression levels in the cerebral cortex neighboring the injection site, where local ASO concentrations were high (Figure 5D). No apparent difference in the density of GFAP- and IBA1-positive cells was identified in pontine nuclei or any other assessed brain region of ASO-2- and ASO-5-treated mice. Qualitatively, however, more GFAP-positive cells were apparent in the pons of ASO-4-treated mice (Figure 5E).

### In Vivo Assessment of ASOs in Q135 SCA3 Transgenic Mice

The top ASO candidates identified in Q84 mice were similarly evaluated in hemizygous Q135 mice, a transgenic model of SCA3 that expresses an *ATXN3* cDNA splice isoform with a 135-CAG repeat expansion.[22] Of the three ASOs demonstrating significant ATXN3 knockdown in brain regions of Q84 mice, only ASO-4 and ASO-5 target sequences are present in the *ATXN3* cDNA transcript expressed in Q135 mice. Thus, only these two ASOs could be evaluated in Q135 mice (Figure 6A).

Sex-matched 8-week-old Q135 mice received a single i.c.v. bolus injection of 500 μg ASO-4, 700 μg ASO-5, 700 μg ASO-Ctrl, or PBS into the right lateral ventricle, and brains were harvested 4 weeks later. The ASO-5 dose was increased to 700 μg to increase potential efficacy, while the ASO-4 dose was maintained at 500 μg due to toxicity concerns from previous Q84 mouse studies. As in the Q84 mouse experiment, Q135 brains were bisected along the midline with the left hemisphere used for protein and RNA analysis and the right hemisphere for immunofluorescence with anti-ASO and anti-ATXN3 antibodies.

Mutant *ATXN3* transcript levels were not significantly reduced in the diencephalon of either ASO-4- or ASO-5-treated mice relative to vehicle or ASO-Ctrl-treated mice, assessed by qRT-PCR (Figure 6B). In contrast, wild-type *ATXN3* transcript levels were significantly reduced ($p < 0.0001$) in ASO-5-treated mice, but not in ASO-4-treated mice, consistent with the conservation of target sequence for ASO-5 but not ASO-4. This reduction in wild-type *Atxn3* transcript levels confirms effective ASO-5 delivery to the diencephalon for targeting

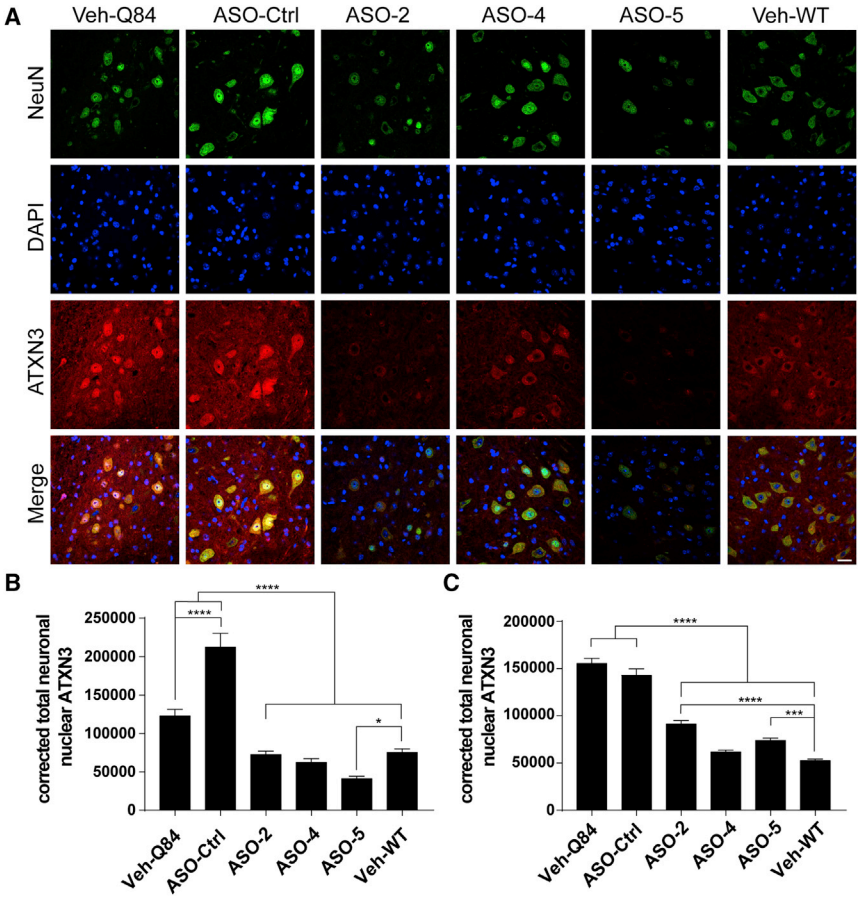


**Figure 4. ASOs Significantly Suppress ATXN3 Accumulation within Neuronal Nuclei**

(A) Representative immunofluorescence images of ATXN3 (red) reduction within neuronal nuclei (NeuN, green; DAPI, blue) in the deep cerebellar nuclei (DCN) of Q84 hemizygous mice, 4 weeks post-treatment. Scale bar represents 25 μm. (B and C) Quantification of total corrected neuronal nuclear ATXN3 fluorescence in the DCN (B) and pontine nuclei (C). Data (mean ± SEM) are reported relative to Q84 vehicle-treated mice (n = 3 per group). One-way ANOVA performed with the post hoc Tukey test (*$p < 0.05$; ***$p < 0.001$; ****$p < 0.0001$).

but also supports a greatly reduced targeting capacity of the ASOs for the cDNA transgene relative to the wild-type gene. Immunoblotting for ATXN3 also revealed no significant difference in mutant ATXN3 levels in the cerebellum of treated mice (Figure 6C).

Anti-ASO immunofluorescence confirmed that ASOs were delivered successfully to the cerebellum and pons of Q135 mice, as in Q84 mice (Figures 6D and 6E). Anti-ATXN3 fluorescence revealed no visible difference in diffuse ATXN3 protein staining or in ATXN3-positive punctate pathology in ASO-4-treated mice relative to ASO-Ctrl- and vehicle-treated mice in the DCN (Figure 6D) or pons (Figure 6E). ASO-5-treated mice exhibited almost total silencing of diffuse ATXN3 staining, which we attribute to efficient knockdown of endogenous murine ATXN3. However, ATXN3-positive punctate neuropathology did not appear markedly reduced in the Q135 pontine nuclei of 12-week-old mice (Figure 6E).

## DISCUSSION

Our studies here strongly support the promise of ASO-mediated targeting of *ATXN3* as a potentially effective therapeutic approach for SCA3. Several tested ASOs were effective in reducing levels of the pathogenic ATXN3 protein both in human disease fibroblasts and in a mouse model expressing the full-length human mutant *ATXN3* gene.

SCA3 brains exhibit widespread degenerative and neuropathological changes, including neuronal loss and gliosis in the DCN, vestibular and other brainstem nuclei, spinocerebellar tracts, substantia nigra, thalamus, and globus pallidus.[26,29] This broad distribution highlights the need for broad targeting of a therapeutic agent to affected brain regions. Here we identified several ASOs that effectively target the full-length *ATXN3* human transcript in SCA3 patient fibroblasts, including exonic, intronic, and 3′-UTR targets. All five ASOs were carried forward in a short-term assessment in the Q84 mouse model of SCA3. Similar to previous ASO studies,[16,30–32] we directly injected ASOs into the lateral ventricle to allow the natural flow of the cerebrospinal fluid to deliver the ASO therapy to affected brain regions of interest. Similar broad ASO delivery throughout the CNS was shown in other rodent models following i.c.v. injection and non-human primates following intrathecal injection in HD ASO studies.[11] Importantly, for three of the five tested ASOs, a single ASO injection into symptomatic Q84 transgenic mice was sufficient to significantly reduce (>50%) ATXN3 protein levels in the cerebellum, diencephalon, and cervical spinal cord. The top ASO candidates also caused a marked reduction in HMW aggregated ATXN3 in the diencephalon, detectable on denaturing gels.

In contrast to the robust suppression in Q84 mice, we failed to observe robust ASO-mediated reduction of mutant ATXN3 in a second transgenic model, the Q135 mouse. This lack of efficacy was not due to insufficient delivery, since ASO-5 reduced endogenous *Atxn3* levels in Q135 mice much as it did in Q84 mice. Decreased potency of ASO targeting in Q135 mice may result from key differences between cDNA-derived and full-length transgenic models of disease. First, the exclusion of any intronic sequences in the ATXN3 transcript of Q135 may significantly alter RNA processing dynamics of the mutant transcript, which could have direct effects on ASO targeting capacity. In addition, Q135 mice express a single isoform of human ATXN3, the mRNA structure of which may be less accessible to ASO binding than other isoforms. In support of this argument, two previous studies investigating ASO therapy for the polyglutamine disease spinal bulbar

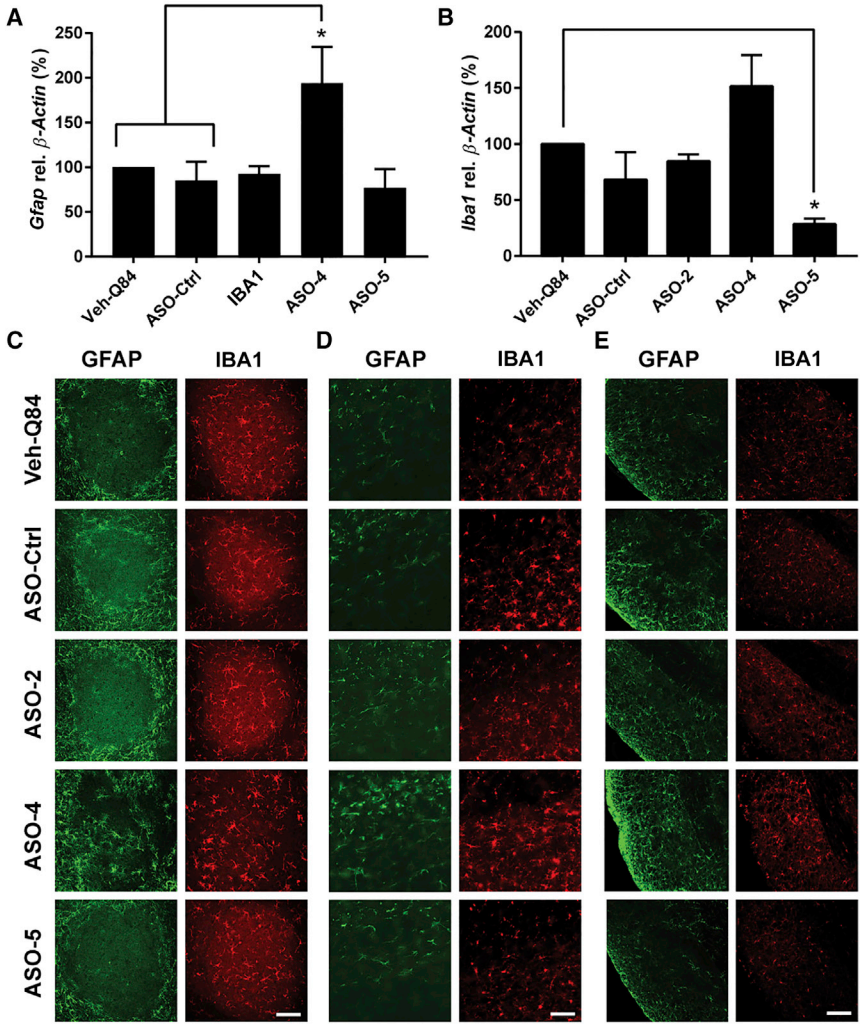


**Figure 5. ASOs Result in Limited Immunoreactive Changes in Q84 Mice**

(A and B) Transcript levels of the astrocytic marker *Gfap* (A) and microglial marker *Iba1* (B) in the left diencephalon of vehicle and ASO-treated mice 4 weeks after injection. Means ± SEM are reported relative to Q84 vehicle-treated mice (n = 6 per group). One-way ANOVA statistical analysis performed with the post hoc Tukey test (*$p < 0.05$). (C–E) Representative GFAP (green) and IBA1 (red) immunofluorescence images of the deep cerebellar nuclei (DCN) (C), cerebral cortex (D), and body of the pons (E). Scale bars represent 100 μm in (C) and (D) and 50 μm in (E).

muscular atrophy (SBMA) noted much less suppression of the targeted transcript in a cDNA transgenic mouse model than in a mouse model of SBMA expressing the full-length gene.[33,34] Future studies could include other biologically relevant models of SCA3 such as recently available knock-in models to further validate ASO potency.[35]

We further assessed the tolerability of the three most effective ASOs in vivo. ASO-2 and ASO-5 proved to be safe and well tolerated, as evidenced by the absence of astrocytic or microglial activation after treatment. ASO-5 even decreased transcript levels of the microglia marker *Iba1* in Q84 mice, suggesting a partial rescue of neuroinflammatory changes that occur in SCA3 patient brains as well as in transgenic SCA3 mouse models.[22,36] In contrast to ASO-2 and ASO-5, ASO-4 caused significant elevation of *Gfap* transcript levels in the diencephalon and increased astrocytic invasion into the DCN. Although ASO-4 was designed to have low off-targeting potential, the apparent toxicity in fibroblast and animal models of disease do not support further development of ASO-4 as a potential therapeutic in SCA3. Importantly, the lack of an overt immune response following endogenous ATXN3 suppression, either in the presence or absence of the human disease protein, supports previous findings that ATXN3 is likely not an essential protein and that non-allele-specific silencing of ATXN3 may be well tolerated as a therapeutic approach.[7,8] Future studies may employ additional in vivo safety and toxicity evaluations, such as transcriptome analysis or stereology in treated SCA3 mice.

The immediate next step is to move the safe and efficacious ASOs, ASO-2 and ASO-5, into a long-term trial to assess their impact on behavioral phenotypes and animal survival. While hemizygous Q84 mice used in these studies express the full-length human *ATXN3* gene, they display relatively subtle behavioral phenotypes.[23] For a long-term trial, we will need to employ homozygous Q84 mice, which recapitulate numerous aspects of the human disease including quantifiable motor deficits, robust aggregate pathology, and early lethality.[3,23] In summary, we have established the first proof of concept for ASO efficacy and tolerability in a SCA3 mouse model of disease.

## MATERIALS AND METHODS

### Animals

All animal procedures were approved by the University of Michigan Committee on the Use and Care of Animals (UCUCA). YACMJD84.2Q-C57BL/6 and CMVMJDQ135-C57BL/6 transgenic mice were housed in cages with a maximum number of five animals and maintained in a standard 12-hr light/dark cycle with food and water ad libitum. Genotyping was performed using DNA isolated from tail biopsy at the time of weaning, as previously described.[23] YACMJD84.2Q transgenic mice hemizygosity was determined by standard PCR using GoTaq Green Master Mix (Promega) to amplify a fragment of the *ATXN3* transgene with primer sequences 5′-TGGCCTTCACATG GATGTGAA and 5′-CCAGTGACTACTTTGATTCG, and normalizing to a genomic fragment of mouse *Atxn3* chromosome 7 with primer sequences 5′-CTCTGTACAGACAGGGAGATGTGAG and 5′-GAGGATGCAAAGGAGCCAAGTGACC. CMVMJDQ135 mouse

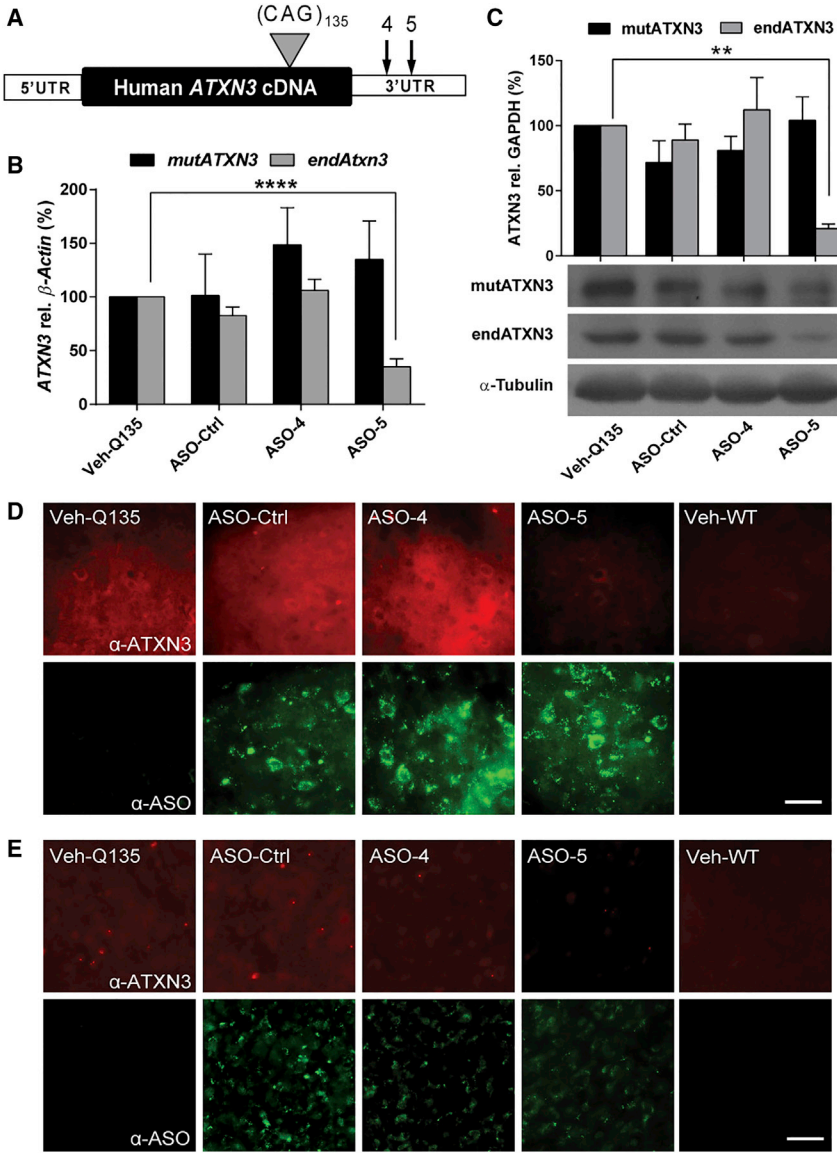


**Figure 6. ASOs Do Not Reduce Mutant ATXN3 Expression in a Second Model, the Q135 cDNA Transgenic Mouse, Despite Effective Delivery**

(A) Schematic of anti-*ATXN3* ASO target sites on the CMV MJD-Q135 *ATXN3* cDNA transcript. (B) Mutant *ATXN3* (*mutATXN3*) and endogenous *Atxn3* (*endAtxn3*) transcript levels in the diencephalon of Q135 mice 4 weeks after injection (n = 6 per group). Data shown are mean ± SEM relative to Q135 vehicle-treated mice (n = 6 per group). One-way ANOVA statistical analysis performed with the post hoc Dunnett test (**$p < 0.01$; ****$p < 0.0001$). (C) Western blotting and quantification of mutant human ATXN3 and endogenous murine ATXN3 expression in Q135 diencephalon 4 weeks after injection. (D and E) Representative ATXN3 (red) and ASO (green) immunofluorescence images of the deep cerebellar nuclei (DCN) (D) and pontine nuclei (E). Scale bars represent 50 μm.

hemizygosity was similarly determined using the CMV primer sequences 5′-GAAGACACCGGGACCGATCCAG and 5′-CCAGAAG GCTGCTGTAAAAACGTGC. The reactions were performed using a T100 thermocycler (Bio-Rad). Genotypes of all studied mice were confirmed using DNA extracted from tails collected postmortem. Animals were euthanized 4 weeks after ASO i.c.v. bolus, anesthetized with 100 mg/kg ketamine per 10 mg/kg xylazine intraperitoneally, and perfused transcardially with PBS.

### ASOs

The five candidate anti-*ATXN3* ASOs and scrambled control ASO used in this study are 18 nucleotides in length with eight unmodified deoxynucleotides with a native sugar-phosphate backbone flanked by five MOE-modified ribonucleotides on the 5′- and 3′-termini with a phosphorothioate backbone. These ASOs were designed to target the intron, exon, or 3′-UTR of human *ATXN3*. Oligonucleotides were synthesized as described previously.[37,38] ASOs were solubilized in PBS (without $Ca^{2+}$ or $Mg^{2+}$).

### Cell Line

SCA3 patient-derived fibroblasts (GM06153) containing an expanded ATXN3 allele (23Q/71Q) were obtained from Coriell Cell Repositories. Fibroblasts were maintained at 37°C and 5% $CO_2$ in DMEM (HyClone) supplemented with 15% fetal bovine serum. HEPG2 cells were obtained from ATCC and maintained in Eagle's minimum essential medium (EMEM) (ATCC) supplemented with 10% FBS, 1% non-essential amino acid (NEAA), and 1% sodium pyruvate.

### Electroporation

HEPG2 cells were electroporated at 165 V in 100 μL media with 20,000 cells/well on the BTX high-throughput electroporation system (Harvard Apparatus). Following electroporation, cells were transferred to a collagen-coated plate and placed in an incubator overnight. Twenty-four hours post-treatment, cells were washed with PBS and then lysed with GTC for RNA purification.

### Transfection

SCA3 patient-derived fibroblasts were plated into 12-well plates at 80,000 cells/well density in supplemented DMEM 2 days prior to transfection. ASO transfections were performed using Lipofectamine LTX with PLUS Reagent (Life Technologies) at a final ASO concentration of 4 μM/well according to the manufacturer's instructions. Cells were harvested 48 hr after transfection in TRIzol (Invitrogen) for RNA analysis or 72 hr after transfection using radioimmunoprecipitation assay (RIPA)

buffer containing protease inhibitors (Complete Mini; Roche Diagnostics) for protein analysis.

#### RNA Isolation and qPCR

Total RNA was isolated from transfected fibroblasts and dissected brain tissue using TRIzol reagent according to the manufacturer's protocol (Invitrogen). Reverse transcription was performed on 1 μg total RNA using the iScript cDNA synthesis kit according to the manufacturer's instructions (Bio-Rad). The cDNA was diluted 1:10 in nuclease-free water. iQ SYBR Green qPCR was performed on the diluted cDNA following the manufacturer's protocol (Bio-Rad). Analysis was performed using average adjusted relative quantification using the following primers: human *ATXN3* (5′-GAAGCTGACCA ACTCCTGC-3′ and 5′-CTTCTAACACTCGTTCCAGG-3′), mouse *Beta Actin* (5′-GAACGGACAGCCATGGGCGGG-3′ and 5′-GTGT GTCCCCAAGCCCCACG-3′), mouse *Gfap* (5′-GAAAACCGCA TCACCATTCC-3′ and 5′-CTTATTGACCTCACCATCCCG-3′), mouse *Iba1* (5′- CCACCGTGTCAGAATCCAC-3′ and 5′-ATGCTG GGCAAGAGATCT-3′), human *GAPDH* (5′-CTCCGGGTGATG CTTTTCCT and 5′-ACATGTAAACCATGTAGTTGAGGT), and mouse *Atxn3* (5′-TGTCTTGTTACAGAAAGATCAG and 5′-GTTA CAAGAACAGAGCTGACT).

#### Immunoblotting

Protein lysates from SCA3 fibroblasts were produced by lysis in RIPA buffer containing protease inhibitors (Complete Mini), followed by centrifugation. Protein lysates from the perfused and dissected mouse forebrain, diencephalon, cerebellum, and cervical spinal cord were produced by lysis and homogenization in RIPA buffer containing protease inhibitors (Complete Mini) via Dounce homogenizers, followed by sonication and centrifugation. Total protein concentrations of extracted supernatants were determined using the bicinchoninic acid (BCA) method (Pierce) and stored at −80°C. A total of 50 μg total mouse brain protein lysate or 5 μg total fibroblast protein lysate was resolved in 10% SDS-polyacrylamide electrophoresis gels and transferred to polyvinylidene difluoride (PVDF) membranes. Membranes were incubated overnight at 4°C with various antibodies: mouse anti-ATXN3 (1H9) (1:1,000, MAB5360; Millipore), rabbit anti-MJD antibody (1:10,000; Paulson et al.[39]), mouse anti-GAPDH (1:5,000, MAB374; Millipore), or rabbit anti-α-tubulin (1:5,000, S2144; Cell Signaling Technology). Bound primary antibodies were visualized by incubation with a peroxidase-conjugated anti-mouse or anti-rabbit secondary antibody (1:10,000; Jackson ImmunoResearch Laboratories) followed by treatment with an enhanced chemiluminescence (ECL)-plus reagent (Western Lighting; PerkinElmer) and exposure to autoradiography films. Band intensities were quantified using ImageJ analysis software (NIH).

#### Stereotaxic Mouse i.c.v. ASO Bolus Delivery

Stereotaxic administration of ASOs into the right lateral ventricle via i.c.v. injections was performed on mice under vaporized isoflurane anesthesia. Eight-week-old mice received a single i.c.v. bolus injection using established protocols.[30] Six sex-matched Q84, Q135, or wild-type littermates were included per experimental treatment group. All treatment groups were blinded to the experimenter prior to analysis. For each injection, a small incision was made, the skull was exposed, and a small burr hole was drilled at the proper coordinates: anterior-posterior, +0.3 mm; mediolateral, −1.0 mm; and dorsoventral, −3.0 mm relative to the bregma. Three minutes after the needle (7758-04; Hamilton) connected to a 10-μL syringe (7653-01; Hamilton) was placed into the proper coordinates, a total of 500–700 μg ASO diluted in 10 μL PBS (without $Ca^{2+}$ or $Mg^{2+}$) was delivered at an infusion rate of 0.5 μL/s using an injection pump (UMC4; World Precision Instruments). For all ASO studies in Q84 mice, mice received 500 μg of the five active ASOs or control ASO. In the Q135 ASO studies, mice received 500 μg ASO-4, 700 μg ASO-5, or 700 μg ASO-Ctrl. Five minutes after the infusion was completed, the needle was retracted at a rate of 1 mm/s. The incision site was sutured with synthetic absorbable sutures (V1D397; Vet One) and the mouse was allowed to recover in a temperature-controlled environment. Following surgery, weight, grooming activity, and home cage activity were recorded for up to 10 days according to UCUCA guidelines.

#### Immunohistochemistry

Whole brains perfused with PBS and the right hemispheres were post-fixed for 48 hr at 4°C in 4% paraformaldehyde solution and immersed in 30% sucrose until saturated, and 40 μm was sagittally sectioned on a sledge microtome (SM200R; Leica Biosystems). Sections were stored in cryoprotectant solution at −20°C until they were processed for immunofluorescence. Brain sections were subjected to a basic antigen retrieval, washed, blocked, and incubated overnight at 4°C in primary antibody supplemented with 0.025% Triton X-100, 0.5% BSA, and 5% serum from the host line for secondary antibodies (donkey or goat). Primary antibodies used in these studies included the following: mouse anti-ATXN3 (1H9) (1:1,000, MAB5360; Millipore), rabbit anti-ASO (1:5,000, Ionis Pharmaceuticals), rabbit anti-NeuN-488 conjugated (1:1,000, ABN78A4; Millipore), mouse anti-GFAP (1:1,000, 3670; Cell Signaling Technology), and rabbit anti-IBA1 (1:1,000, 019-19741; Wako Chemicals). Primary incubated sections were then washed and incubated with the corresponding secondary Alexa Fluor 488 or 568 antibodies (1:1,000; Invitrogen). All sections were stained with DAPI (Sigma) for 15 min at room temperature, mounted with Prolong Gold Antifade Reagent (Invitrogen), and imaged using an IX71 Olympus inverted microscope or Nikon-A1 confocal microscope. NeuN-positive ATXN3 nuclear accumulation was calculated using ImageJ software. Corrected total neuronal nuclear ATXN3 fluorescence = (nuclear area × mean ATXN3 fluorescence) – (nuclear area × mean fluorescence of background readings).

## AUTHOR CONTRIBUTIONS

Conceptualization, L.R.M, G.R., G.H., H.B.K., H.L.P., H.S.M.; Methodology, L.R.M, G.R., H.B.K., H.S.M.; Investigation, L.R.M, G.R., I.T.D., M.Q., K.G.B., D.G., H.S.M.; Writing, L.R.M, G.R., H.B.K., H.L.P., H.S.M.; Funding Acquisition, L.R.M, G.R., H.L.P., H.S.M.; Supervision, G.H., H.B.K.; H.L.P., H.S.M.

## CONFLICTS OF INTEREST

D.G., G.H., and H.B.K. are employees of Ionis Pharmaceuticals. This work was supported in part by Ionis Pharmaceuticals.

## ACKNOWLEDGMENTS

We thank Dr. Patricia Maciel for providing the CMVMJD-Q135 mouse model. Ionis Pharmaceutics identified and generated the anti-*ATXN3* ASOs. This work was supported in part by a research contract from Ionis Pharmaceuticals (to H.L.P.), a National Ataxia Foundation Postdoctoral Fellowship Award (to G.R.), a grant from the NIH National Center for Advancing Translational Sciences (UL1-TR000433 to G.R.), a Michigan Brain Initiative Predoctoral Fellowship for Neuroscience (to L.R.M.), a Becky Babcox Fund Pilot Research Award (G015616 to principal investigator [PI] H.S.M.), and grants from the NIH (T32-NS007222-33 to H.S.M. and R01-NS038712 to PI H.L.P.).

## REFERENCES

1. Costa, Mdo.C., and Paulson, H.L. (2012). Toward understanding Machado-Joseph disease. Prog. Neurobiol. *97*, 239–257.
2. Alves, S., Nascimento-Ferreira, I., Auregan, G., Hassig, R., Dufour, N., Brouillet, E., Pedroso de Lima, M.C., Hantraye, P., Pereira de Almeida, L., and Déglon, N. (2008). Allele-specific RNA silencing of mutant ataxin-3 mediates neuroprotection in a rat model of Machado-Joseph disease. PLoS ONE *3*, e3341.
3. Costa, Mdo.C., Luna-Cancalon, K., Fischer, S., Ashraf, N.S., Ouyang, M., Dharia, R.M., Martin-Fishman, L., Yang, Y., Shakkottai, V.G., Davidson, B.L., et al. (2013). Toward RNAi therapy for the polyglutamine disease Machado-Joseph disease. Mol. Ther. *21*, 1898–1908.
4. Rodriguez-Lebron, E., Costa Mdo, C., Luna-Cancalon, K., Peron, T.M., Fischer, S., Boudreau, R.L., Davidson, B.L., and Paulson, H.L. (2013). Silencing mutant ATXN3 expression resolves molecular phenotypes in SCA3 transgenic mice. Mol. Ther. *21*, 1909–1918.
5. Nóbrega, C., Nascimento-Ferreira, I., Onofre, I., Albuquerque, D., Hirai, H., Déglon, N., and de Almeida, L.P. (2013). Silencing mutant ataxin-3 rescues motor deficits and neuropathology in Machado-Joseph disease transgenic mice. PLoS ONE *8*, e52396.
6. Evers, M.M., Tran, H.D., Zalachoras, I., Pepers, B.A., Meijer, O.C., den Dunnen, J.T., van Ommen, G.J., Aartsma-Rus, A., and van Roon-Mom, W.M. (2013). Ataxin-3 protein modification as a treatment strategy for spinocerebellar ataxia type 3: removal of the CAG containing exon. Neurobiol. Dis. *58*, 49–56.
7. Schmitt, I., Linden, M., Khazneh, H., Evert, B.O., Breuer, P., Klockgether, T., and Wuellner, U. (2007). Inactivation of the mouse Atxn3 (ataxin-3) gene increases protein ubiquitination. Biochem. Biophys. Res. Commun. *362*, 734–739.
8. Boy, J., Schmidt, T., Wolburg, H., Mack, A., Nuber, S., Böttcher, M., Schmitt, I., Holzmann, C., Zimmermann, F., Servadio, A., and Riess, O. (2009). Reversibility of symptoms in a conditional mouse model of spinocerebellar ataxia type 3. Hum. Mol. Genet. *18*, 4282–4295.
9. Seidel, K., Siswanto, S., Brunt, E.R., den Dunnen, W., Korf, H.W., and Rüb, U. (2012). Brain pathology of spinocerebellar ataxias. Acta Neuropathol. *124*, 1–21.
10. Cerritelli, S.M., and Crouch, R.J. (2009). Ribonuclease H: the enzymes in eukaryotes. FEBS J. *276*, 1494–1505.
11. Kordasiewicz, H.B., Stanek, L.M., Wancewicz, E.V., Mazur, C., McAlonis, M.M., Pytel, K.A., Artates, J.W., Weiss, A., Cheng, S.H., Shihabuddin, L.S., et al. (2012). Sustained therapeutic reversal of Huntington's disease by transient repression of huntingtin synthesis. Neuron *74*, 1031–1044.
12. Passini, M.A., Bu, J., Richards, A.M., Kinnecom, C., Sardi, S.P., Stanek, L.M., Hua, Y., Rigo, F., Matson, J., Hung, G., et al. (2011). Antisense oligonucleotides delivered to the mouse CNS ameliorate symptoms of severe spinal muscular atrophy. Sci. Transl. Med. *3*, 72ra18.
13. Hua, Y., Sahashi, K., Rigo, F., Hung, G., Horev, G., Bennett, C.F., and Krainer, A.R. (2011). Peripheral SMN restoration is essential for long-term rescue of a severe spinal muscular atrophy mouse model. Nature *478*, 123–126.
14. Chiriboga, C.A., Swoboda, K.J., Darras, B.T., Iannaccone, S.T., Montes, J., De Vivo, D.C., Norris, D.A., Bennett, C.F., and Bishop, K.M. (2016). Results from a phase 1 study of nusinersen (ISIS-SMN(Rx)) in children with spinal muscular atrophy. Neurology *86*, 890–897.
15. Miller, T.M., Pestronk, A., David, W., Rothstein, J., Simpson, E., Appel, S.H., Andres, P.L., Mahoney, K., Allred, P., Alexander, K., et al. (2013). An antisense oligonucleotide against SOD1 delivered intrathecally for patients with SOD1 familial amyotrophic lateral sclerosis: a phase 1, randomised, first-in-man study. Lancet Neurol. *12*, 435–442.
16. Lagier-Tourenne, C., Baughn, M., Rigo, F., Sun, S., Liu, P., Li, H.R., Jiang, J., Watt, A.T., Chun, S., Katz, M., et al. (2013). Targeted degradation of sense and antisense C9orf72 RNA foci as therapy for ALS and frontotemporal degeneration. Proc. Natl. Acad. Sci. USA *110*, E4530–E4539.
17. Hu, J., Matsui, M., Gagnon, K.T., Schwartz, J.C., Gabillet, S., Arar, K., Wu, J., Bezprozvanny, I., and Corey, D.R. (2009). Allele-specific silencing of mutant huntingtin and ataxin-3 genes by targeting expanded CAG repeats in mRNAs. Nat. Biotechnol. *27*, 478–484.
18. Hu, J., Gagnon, K.T., Liu, J., Watts, J.K., Syeda-Nawaz, J., Bennett, C.F., Swayze, E.E., Randolph, J., Chattopadhyaya, J., and Corey, D.R. (2011). Allele-selective inhibition of ataxin-3 (ATX3) expression by antisense oligomers and duplex RNAs. Biol. Chem. *392*, 315–325.
19. Aiba, Y., Hu, J., Liu, J., Xiang, Q., Martinez, C., and Corey, D.R. (2013). Allele-selective inhibition of expression of huntingtin and ataxin-3 by RNA duplexes containing unlocked nucleic acid substitutions. Biochemistry *52*, 9329–9338.
20. Evers, M.M., Pepers, B.A., van Deutekom, J.C., Mulders, S.A., den Dunnen, J.T., Aartsma-Rus, A., van Ommen, G.J., and van Roon-Mom, W.M. (2011). Targeting several CAG expansion diseases by a single antisense oligonucleotide. PLoS ONE *6*, e24308.
21. Toonen, L.J., Schmidt, I., Luijsterburg, M.S., van Attikum, H., and van Roon-Mom, W.M. (2016). Antisense oligonucleotide-mediated exon skipping as a strategy to reduce proteolytic cleavage of ataxin-3. Sci. Rep. *6*, 35200.
22. Silva-Fernandes, A., Costa, Mdo.C., Duarte-Silva, S., Oliveira, P., Botelho, C.M., Martins, L., Mariz, J.A., Ferreira, T., Ribeiro, F., Correia-Neves, M., et al. (2010). Motor uncoordination and neuropathology in a transgenic mouse model of Machado-Joseph disease lacking intranuclear inclusions and ataxin-3 cleavage products. Neurobiol. Dis. *40*, 163–176.
23. Cemal, C.K., Carroll, C.J., Lawrence, L., Lowrie, M.B., Ruddle, P., Al-Mahdawi, S., King, R.H., Pook, M.A., Huxley, C., and Chamberlain, S. (2002). YAC transgenic mice carrying pathological alleles of the MJD1 locus exhibit a mild and slowly progressive cerebellar deficit. Hum. Mol. Genet. *11*, 1075–1094.
24. Bennett, C.F., and Swayze, E.E. (2010). RNA targeting therapeutics: molecular mechanisms of antisense oligonucleotides as a therapeutic platform. Annu. Rev. Pharmacol. Toxicol. *50*, 259–293.
25. Yu, R.Z., Geary, R.S., Monteith, D.K., Matson, J., Truong, L., Fitchett, J., and Levin, A.A. (2004). Tissue disposition of 2′-O-(2-methoxy) ethyl modified antisense oligonucleotides in monkeys. J. Pharm. Sci. *93*, 48–59.
26. Rüb, U., Schöls, L., Paulson, H., Auburger, G., Kermer, P., Jen, J.C., Seidel, K., Korf, H.W., and Deller, T. (2013). Clinical features, neurogenetics and neuropathology of the polyglutamine spinocerebellar ataxias type 1, 2, 3, 6 and 7. Prog. Neurobiol. *104*, 38–66.
27. Riess, O., Rüb, U., Pastore, A., Bauer, P., and Schöls, L. (2008). SCA3: neurological features, pathogenesis and animal models. Cerebellum *7*, 125–137.
28. Haacke, A., Broadley, S.A., Boteva, R., Tzvetkov, N., Hartl, F.U., and Breuer, P. (2006). Proteolytic cleavage of polyglutamine-expanded ataxin-3 is critical for aggregation and sequestration of non-expanded ataxin-3. Hum. Mol. Genet. *15*, 555–568.
29. Rosenberg, R.N. (1992). Machado-Joseph disease: an autosomal dominant motor system degeneration. Mov. Disord. *7*, 193–203.
30. DeVos, S.L., and Miller, T.M. (2013). Direct intraventricular delivery of drugs to the rodent central nervous system. J. Vis. Exp. *75*, e50326.

31. Østergaard, M.E., Southwell, A.L., Kordasiewicz, H., Watt, A.T., Skotte, N.H., Doty, C.N., Vaid, K., Villanueva, E.B., Swayze, E.E., Bennett, C.F., et al. (2013). Rational design of antisense oligonucleotides targeting single nucleotide polymorphisms for potent and allele selective suppression of mutant Huntingtin in the CNS. Nucleic Acids Res. *41*, 9634–9650.

32. Southwell, A.L., Skotte, N.H., Kordasiewicz, H.B., Østergaard, M.E., Watt, A.T., Carroll, J.B., Doty, C.N., Villanueva, E.B., Petoukhov, E., Vaid, K., et al. (2014). In vivo evaluation of candidate allele-specific mutant huntingtin gene silencing antisense oligonucleotides. Mol. Ther. *22*, 2093–2106.

33. Lieberman, A.P., Yu, Z., Murray, S., Peralta, R., Low, A., Guo, S., Yu, X.X., Cortes, C.J., Bennett, C.F., Monia, B.P., et al. (2014). Peripheral androgen receptor gene suppression rescues disease in mouse models of spinal and bulbar muscular atrophy. Cell Rep. *7*, 774–784.

34. Sahashi, K., Katsuno, M., Hung, G., Adachi, H., Kondo, N., Nakatsuji, H., Tohnai, G., Iida, M., Bennett, C.F., and Sobue, G. (2015). Silencing neuronal mutant androgen receptor in a mouse model of spinal and bulbar muscular atrophy. Hum. Mol. Genet. *24*, 5985–5994.

35. Ramani, B., Harris, G.M., Huang, R., Seki, T., Murphy, G.G., Costa, Mdo.C., Fischer, S., Saunders, T.L., Xia, G., McEachin, R.C., and Paulson, H.L. (2015). A knockin mouse model of spinocerebellar ataxia type 3 exhibits prominent aggregate pathology and aberrant splicing of the disease gene transcript. Hum. Mol. Genet. *24*, 1211–1224.

36. Evert, B.O., Vogt, I.R., Kindermann, C., Ozimek, L., de Vos, R.A., Brunt, E.R., Schmitt, I., Klockgether, T., and Wüllner, U. (2001). Inflammatory genes are upregulated in expanded ataxin-3-expressing cell lines and spinocerebellar ataxia type 3 brains. J. Neurosci. *21*, 5389–5396.

37. Cheruvallath, Z.S., Kumar, R.K., Rentel, C., Cole, D.L., and Ravikumar, V.T. (2003). Solid phase synthesis of phosphorothioate oligonucleotides utilizing diethyldithiocarbonate disulfide (DDD) as an efficient sulfur transfer reagent. Nucleosides Nucleotides Nucleic Acids *22*, 461–468.

38. McKay, R.A., Miraglia, L.J., Cummins, L.L., Owens, S.R., Sasmor, H., and Dean, N.M. (1999). Characterization of a potent and specific class of antisense oligonucleotide inhibitor of human protein kinase C-alpha expression. J. Biol. Chem. *274*, 1715–1722.

39. Paulson, H.L., Das, S.S., Crino, P.B., Perez, M.K., Patel, S.C., Gotsdiner, D., Fischbeck, K.H., and Pittman, R.N. (1997). Machado-Joseph disease gene product is a cytoplasmic protein widely expressed in brain. Ann Neurol. *41*, 453–462.